6618 *Biochemistry* **2009,** *48,* 6618–6623
DOI: 10.1021/bi900838d

BIOCHEMISTRY
including biophysical chemistry & molecular biology
*Article*

# Projection Structure by Single-Particle Electron Microscopy of Secondary Transport Proteins GltT, CitS, and GltS

Katarzyna B. Mościcka,[‡,∥] Tomasz Krupnik,[∥,§] Egbert J. Boekema,*[,‡] and Juke S. Lolkema*[,§]

[‡]*Biophysical Chemistry and* [§]*Molecular Microbiology, Groningen Biomolecular Sciences and Biotechnology Institute, University of Groningen, Groningen, The Netherlands.* [∥]*These authors contributed equally to this study*

*Received May 18, 2009; Revised Manuscript Received June 10, 2009*

ABSTRACT: The structure of three secondary transporter proteins, GltT of *Bacillus stearothermophilus*, CitS of *Klebsiella pneumoniae*, and GltS of *Escherichia coli*, was studied. The proteins were purified to homogeneity in detergent solution by $Ni^{2+}$-NTA affinity chromatography, and the complexes were determined by BN-PAGE to be trimeric, dimeric, and dimeric for GltT, CitS, and GltS, respectively. The subunit stoichiometry correlated with the binding affinity of the $Ni^{2+}$-NTA resin for the protein complexes. Projection maps of negatively stained transporter particles were obtained by single-particle electron microscopy. Processing of the GltT particles revealed a projection map possessing 3-fold rotational symmetry, in good agreement with the trimer observed in the crystal structure of a homologous protein, $Glt_{Ph}$ of *Pyrococcus horikoshii*. The CitS protein showed up in two main views: as a kidney-shaped particle and a biscuit-shaped particle, both with a long axis of 160 Å. The latter has a width of 84 Å, the former of 92 Å. Symmetry considerations identify the biscuit shape as a top view and the kidney shape as a side view from within the membrane. Combining the two images shows that the CitS dimer is a protein with a strong curvature at one side of the membrane and, at the opposite side, an indentation in the middle at the subunit interface. The GltS protein was shaped like CitS with dimensions of 145 Å × 84 Å. The shapes and dimensions of the CitS and GltS particles are consistent with a similar structure of these two unrelated proteins.

Secondary transporters use the free energy stored in ion and/or solute gradients to drive the transport of a solute across the cytoplasmic or internal membranes of biological cells. They are widely spread throughout all kingdoms of life; they are found in every biological cell, and a specific transporter protein can probably be found for every low-molecular weight compound in nature. Their high abundance is reflected in the great diversity of sequences encoding secondary transporters. The transporter classification (TC)[1] system developed in the Saier laboratory lists some 95 different gene (super)families encoding secondary transporters (subclass TC 2.A) (*1*). Significant progress made during the past decade in determining high-resolution X-ray structures of secondary transporters (*2*−*10*) suggests that the phylogenetic diversity correlates with a similar diversity in three-dimensional structure and translocation mechanism, emphasizing the need for less elaborate methods for low-resolution structure determination of these proteins.

*To whom correspondence should be addressed. E.J.B.: Nijenborgh 4, 9747 AG Groningen, The Netherlands; telephone, +31 50 363 4225; fax, +31 50 363 4800; e-mail, e.j.boekema@rug.nl. J.S.L.: Biological Center, Kerklaan 30, 9751NN Haren, The Netherlands; telephone, +31 50 363 2155; fax, +31 50 363 2154; e-mail, j.s.lolkema@rug.nl.

[1]Abbreviations: TC, transporter classification; EM, electron microscopy; DAACS, dicarboxylate/amino acid cation symporter; 2HCT, 2-hydroxycarboxylate transporter; ESS, glutamate solute symporter; DDM, β-dodecyl maltoside.

Single-particle analysis of electron microscopy (EM) projections is a simple and attractive method for studying the structure of (membrane) proteins if applied to negatively stained specimens with a mass between ∼100 and 2000 kDa. Many thousands of projections can be processed within a short time, which is necessary to obtain high-quality two-dimensional projection maps. Over the last 25 years, single-particle averaging has become a well-established technique for obtaining information at a medium resolution (10−20 Å) and to near-atomic resolution for some highly symmetric objects (*11*, *12*). In the case of membrane proteins, the resolution is often lower because the particles are surrounded by a nonstructured detergent boundary layer.

In this study, the projection structure of three secondary transporters, GltT, CitS, and GltS, is studied using single-particle electron microscopy. The transporters belong to different gene families, suggesting different structures. The $H^+$-glutamate symporter GltT of *Bacillus stearothermophilus* is a member of the dicarboxylate/amino acid cation symporter (DAACS) family (*13*). The DAACS family is found in all kingdoms of life and includes transporters found in neurons and glial cells in the mammalian central nervous system. A member of the family, $Glt_{Ph}$ of *Pyrococcus horikoshii*, has been crystallized, and the three-dimensional structure was determined at a resolution of 2.69 Å (*5*) . CitS of *Klebsiella pneumoniae* transports citrate in

 Published on Web 06/11/2009 

symport with two sodium ions and one proton. CitS belongs to the family of 2-hydroxycarboxylate transporters (2HCT) that contains transporters exclusively found in bacteria (*14*). GltS of *Escherichia coli* transports glutamate in symport with $Na^+$ ions (*15*−*17*) . GltS belongs to the glutamate sodium symporter (ESS) family, another bacterial family of transporters. In spite of the apparently different evolutionary origin of the CitS and GltS proteins, they have been proposed to share a similar structure by hydropathy profile analysis (*18*, *19*), and evidence of this has been published (*20*, *21*).

The transporter proteins are expected to be at the lower size limit of what is feasible for single-particle EM which has been widely applied in gathering two- and three-dimensional structure information of proteins with a mass of well above 50 kDa. With molecular masses for the polypeptides that form GltT, CitS, and GltS between 42 and 48 kDa, much may depend on the subunit structure. GltT is believed to be a trimer (*22*, *23*) and CitS a dimer (*24*−*26*). Thus, these transporter proteins are of interest for exploration of the possibilities of single-particle electron microscopy for small-sized membrane proteins. It is demonstrated here that the projection structure of GltT is in good agreement with the X-ray structure of the homologous protein $Glt_{Ph}$ (*5*) showing that for these small membrane proteins relevant structural information can be obtained by the technique. Projection structures of CitS and GltS are consistent with a dimeric structure, and a model is presented for the shape of the CitS dimer sitting in the membrane.

## EXPERIMENTAL PROCEDURES

*Cell Growth and Genetic Constructs*. *E. coli* strain DH5α was used as a host to express the transporter proteins and derivatives. Plasmids pGltThis (*27*) encoding glutamate transporter GltT of *B. stearothermophilus*, pBADCitS (*28*) encoding citrate transporter CitS of *K. pneumoniae*, and pBADGltS (*20*) encoding glutamate transporter GltS of *E. coli* were described before. Freshly transformed bacteria were used to inoculate an overnight growing preculture. Twenty-five milliliters of preculture was added to 1 L of Luria Broth (LB) medium at 37 °C containing 50 μg/mL ampicillin (Roche Diagnostic GmbH, Manninheim, Germany) under continuous shaking (200 rpm). At an $OD_{660}$ of 0.6, 0.1% arabinose (Sigma-Aldrich GmbH, Steinheim, Germany) was added to induce expression of the transporters, after which the culture was allowed to grow for an additional 1 h. Subsequently, cells were harvested by being spun at 8000 rpm for 10 min at 4 °C, washed with 50 mL of 50 mM $KP_i$ (pH 7) at 4 °C, and resuspended in 5 mL of the same buffer.

*Purification of Transporter Proteins*. Cells from a 1 L culture resuspended in 10 mL of 50 mM $KP_i$ (pH 7) containing 1 μg/mL DNase were passed three times through a pressure cell disrupter at 13500 psi and 4 °C. Following a low spin at 8000 rpm for 10 min at 4 °C to remove debris and unbroken cells, the supernatant was centrifuged at 80000 rpm for 25 min at 4 °C (high spin). The membrane fraction was resuspended and washed once with 50 mM $KP_i$ buffer (pH 7) containing 1 M NaCl. The membranes were resuspended in 1 mL of 50 mM $KP_i$ buffer (pH 7) and stored in liquid $N_2$ until they were used.

Transporter proteins were solubilized from the membranes by partial extraction. Membranes were incubated for 1 h at 4 °C under continuous shaking in 50 mM $KP_i$ buffer (pH 7) containing 400 mM NaCl, 10% glycerol, and 0.5% β-dodecyl maltoside (DDM). Undissolved membrane material which contained the transporter proteins was recovered by being spun at 80000 rpm for 25 min at 4 °C. The extraction procedure was repeated with the same buffer with 1% Triton X-100 instead of DDM. After being spun, the supernatant was passed through a 0.2 μm filter, made 20 mM in imidazole, and applied to a 1 mL bed volume $Ni^{2+}$-NTA column (HisTrap HP) mounted in an ACTA HPLC system. Previously, the column had been conditioned for 5 min at a flow rate of 1 mL/min with a 50 mM $KP_i$ buffer (pH 8) containing 600 mM NaCl, 10% glycerol, 0.03% DDM, and 20 mM imidazole. The column was washed with 10 mL of 50 mM $KP_i$ buffer (pH 7) containing 600 mM NaCl, 10% glycerol, 0.03% DDM, and 50 mM imidazole, after which the proteins were eluted with a linear gradient from 50 to 400 mM imidazole in the same buffer. The $OD_{280}$ of the eluate was measured continuously followed by collection in fractions of 0.5 mL. Fractions were concentrated by ultrafiltration (Centriprep, Millipore) using filters with a cutoff of 30 kDa and analyzed by sodium dodecyl sulfate−polyacrylamide gel electrophoresis (SDS−PAGE) as described previously (*29*) using a 12% acrylamide gel and by Blue Native PAGE (*30*) using a six-step gradient from 8 to 18% acrylamide. The protein concentration was determined from the absorption at 280 nm using extinction coefficients of 43110, 32608, and 28880 $M^{-1}$ $cm^{-1}$ calculated from the CitS, GltS, and GltT amino acid sequences, respectively.

*Electron Microscopy and Single-Particle Analysis*. Negatively stained specimens of GltT, CitS, and GltS were prepared with 2% uranyl acetate on glow-discharged carbon-coated copper grids. Electron microscopy was performed on a Philips CM12 electron microscope operated at 120 kV. Images were recorded with a Gatan 4K slow-scan CCD camera at 100000× magnification with a pixel size (after binning the images) of 3.0 Å at the specimen level, with "GRACE" software for semiautomated specimen selection and data acquisition. Approximately 5000, 80000, and 30000 single-particle projections were selected for GltT, CitS, and GltS, respectively. Single-particle analysis was performed with the Groningen Image Processing (GRIP) software package on a personal computer cluster. Selected single-particle projections (96 × 96 pixel frame) were aligned by a multi-reference alignment and reference-free alignment procedures as described previously (*12*, *31*). Next, particles were subjected to multivariate statistical analysis, followed by hierarchical ascendant classification (*12*). After several cycles of multireference alignments, statistical analysis, and classification, the best projections from each set were averaged. In the final classification, 10−20 classes were made. Bad classes were removed, and the remaining classes were further grouped. For GltT, CitS, and GltS, approximately 20, 50, and 50% of the images were finally summed, respectively. The resolution of the class averages was measured by Fourier ring correlation (*32*).

## RESULTS

*Binding Affinity of His-Tagged GltS, CitS, and GltT Proteins for $Ni^{2+}$-NTA Resin*. Depending on the multimeric state of a His-tagged protein, the complex will contain one or more His tags and, therefore, bind more or less strongly to $Ni^{2+}$-NTA resin. Three secondary transporter proteins, GltT of *B. stearothermophilus*, CitS of *K. pneumoniae*, and GltS of *E. coli*, were expressed in *E. coli* DH5α harboring plasmids pGltThis (*27*), pBADCitS (*28*), and pBADGltS (*20*), respectively. The plasmids encode the transport proteins with N-terminal $His_6$ tags. The transporters were solubilized from the membrane by partial

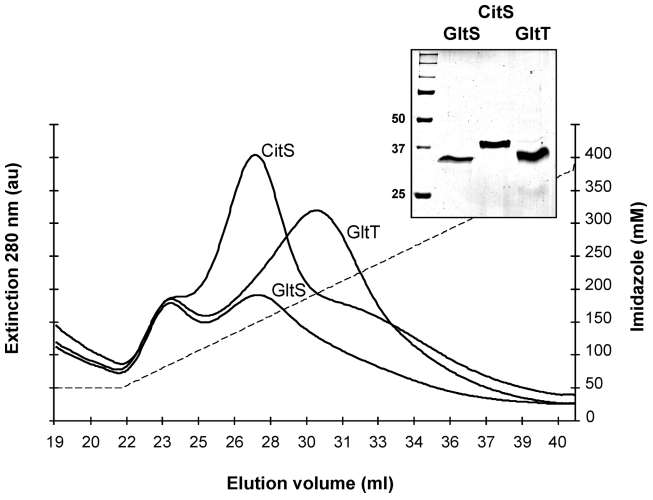


FIGURE 1: $Ni^{2+}$ affinity chromatography purification of GltS, CitS, and GltT. The main plot shows the elution profiles of GltS, CitS, and GltT as measured by the extinction at 280 nm in the eluate. The dashed line indicates the imidazole gradient. The inset shows SDS−PAGE of purified GltS, CitS, and GltT as indicated. Fractions of 1 mL collected at elution volumes of 26−29 mL for CitS and GltS and 30−33 mL for GltT were pooled and concentrated by ultrafiltration before analysis by SDS−PAGE. Estimated molecular masses were 35, 40, and 36 kDa, respectively. The left lane contained marker proteins of 50, 37, and 25 kDa as indicated. The gel was stained with Coomassie Brilliant Blue.

extraction using the detergents DDM and Triton X-100 as described in Experimental Procedures. Solubilized proteins were loaded onto a $Ni^{2+}$-NTA affinity column, and after the column had been washed, bound proteins were eluted from the column by a linear imidazole gradient ranging from 50 to 400 mM (Figure 1). Protein in the eluent was detected by the extinction at 280 nm, and the fractions were assayed for the presence of the transporter proteins by SDS−PAGE. The staining intensity of the proteins in the fractions correlated with the extinction peaks indicated in Figure 1. The GltS and CitS proteins eluted at more or less the same imidazole concentration of 120 mM, while the GltT protein clearly bound more strongly to the resin, eluting at 200 mM imidazole. While other explanations cannot be excluded, the elution profiles might suggest that GltT is in a higher association state than GltS and CitS. The latter two would be in the same association state.

SDS−PAGE following pooling of the peak fractions and concentration by ultrafiltration showed that the procedure resulted in highly pure protein preparations (Figure 1, inset) that were used for the subsequent experiments. The apparent molecular masses of GltS, CitS, and GltT were 35, 40, and 36 kDa, respectively (Table 1). Integral membrane proteins are known to have a mobility higher than expected from their calculated molecular mass because they on average bind more SDS than the soluble proteins used to calibrate the gel. The yield of the procedure, which largely reflects the different levels of expression in the *E. coli* host strain, were 0.083, 0.3, and 0.21 mg of protein/L of cell culture for GltS, CitS, and GltT, respectively.

*Blue Native PAGE of Purified GltS, CitS, and GltT Proteins*. Purified GltS, CitS, and GltT proteins were analyzed by nondenaturing BN-PAGE. Relative mobilities decreased in the following order: GltS > CitS > GltT (Figure 2). Apparent molecular masses of the major protein bands were estimated to be 150, 160, and 180 kDa for GltS, CitS, and GltT, respectively (Table 1). Using a factor of 1.8 to correct for the aberrant

Table 1: PAGE Analyses of GltS, CitS, and GltT Proteins

| | molecular mass (kDa) | | | | |
|---|---|---|---|---|---|
| | | | BN-PAGE | | |
| transporter | sequence[a] | SDS−PAGE | experiment | corrected[b] | state |
| GltS | 43.5 | 35 | 166 | 92 | dimer |
| CitS | 49.1 | 40 | 175 | 97 | dimer |
| GltT | 46.6 | 36 | 229 | 127 | trimer |

[a] Including His tag and/or enterokinase site. [b] See ref *25*.

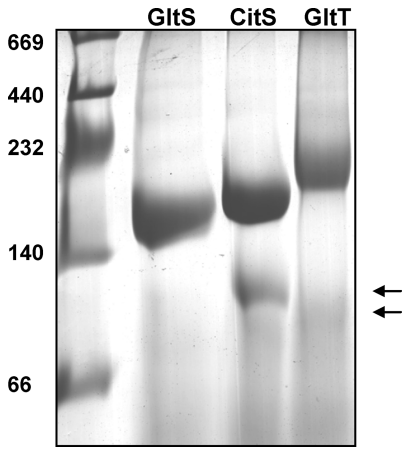


FIGURE 2: BN-PAGE of GltS, CitS, and GltT proteins. The three top fractions of the elution profile obtained after purification by $Ni^{2+}$ affinity chromatography (see Figure 1) were concentrated to 1.0, 0.83, and 0.60 mg/mL for GltS, CitS, and GltT, respectively. An aliquot of 30 $\mu$L was loaded onto the gel. The numbers at the left refer to the molecular masses of the calibration proteins in the first lane in kilodaltons. Arrows at the right point at monomeric CitS and GltT. The gel was stained with Coomassie Brilliant Blue.

mobility behavior of membrane proteins relative to the soluble marker proteins (*25*), these numbers convert to 92, 97, and 127 kDa (Table 1). With calculated molecular masses of the His-tagged proteins of 43.5, 49.1, and 46.6 kDa for GltS, CitS, and GltT, respectively, it follows that the GltS and CitS proteins are dimeric and GltT is trimeric, which is in line with the binding affinities of the proteins for $Ni^{2+}$-NTA resin demonstrated above and previous observations for the CitS and GltT proteins. The glutamate transporter GltT of *B. stearothermophilus* solubilized in detergent was shown to be a homotrimer by chemical cross-linking (*22*). Moreover, the high-resolution crystal structure of the homologous transporter $Glt_{Ph}$ of the archaeon *P. horikoshii* reveals a homotrimeric complex (*5*). Several lines of evidence indicate that CitS of *K. pneumoniae* is a dimeric protein in detergent solution (reviewed in ref *14*).

Minor protein bands with higher mobility were observed after BN-PAGE for CitS and GltT (Figure 2, arrows). In agreement with their calculated molecular masses and since no degradation products were observed via SDS−PAGE of the same samples (Figure 1, inset), these bands are likely to represent small fractions of monomeric CitS and GltT. No dimeric GltT was observed, suggesting that this state of the protein is not stable.

*EM Analysis of CitS, GltS, and GltT Proteins*. Purified GltT, CitS, and GltS transporter proteins were examined by electron microscopy (EM). Large numbers of monodisperse particles of negatively stained GltT, CitS, and GltS proteins were analyzed by single-particle analysis. The final class sums shown in

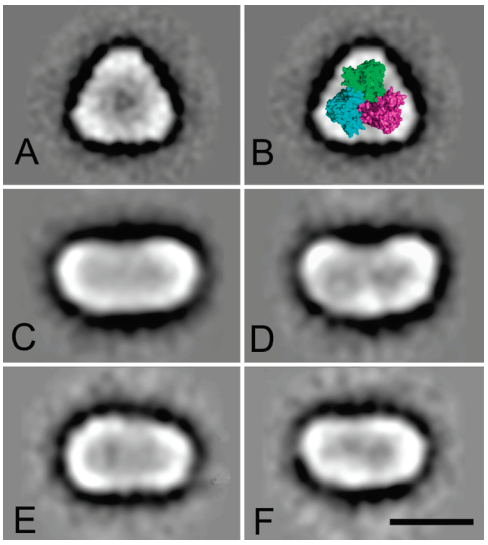


FIGURE 3: Single-particle analysis of GltS, CitS, and GltT. (A) Averaged top view projection of GltT of *B. stearothermophilus* of a total of 5000 particles. (B) Overlay of a space filling model of the high-resolution X-ray structure of $Glt_{Ph}$ of *P. horikoshii* viewed along an axis perpendicular to the membrane on the averaged projection image of GltT shown in panel A. The three protomers of the $Glt_{Ph}$ trimer are indicated in different colors. (C and D) Averaged top view (C) and side view (D) projections of CitS of *K. pneumoniae* based on a total of 80000 particles. (E and F) Averaged projections of GltS of *E. coli* based on a total of 30000 particles. The space bar is 100 Å.

Figure 3 were obtained after several cycles of multireference alignment, multivariate statistical analysis, and classification.

*(i) GltT*. The averaged EM projection maps of negatively stained GltT in detergent solution indicated high numbers of particles showing 3-fold symmetry. The dominant projection image obtained after single-particle averaging was a triangular particle with a base of 118 Å and a clear 3-fold rotational symmetry at ~14 Å resolution (Figure 3A). The 3-fold symmetry points to a trimeric structure of the GltT protein complex. The high-resolution X-ray structure of the homologous transporter $Glt_{Ph}$ resolved previously (*5*) shows a similar 3-fold symmetry when viewed along an axis perpendicular to the membrane (Figure 3B), indicating that the projection structure represents a similar top view. The space filling model based on the X-ray structure of $Glt_{Ph}$ superimposed on the image is a bit smaller than the projection structure which is due to the fact that solubilized membrane proteins are surrounded by a detergent layer, which is not penetrated by the negatively charged stain (*33*). The EM analysis of GltT presented here demonstrates that the shape of integral membrane proteins as small as ~140 kDa can be successfully determined by electron microscopy.

*(ii) CitS*. Analysis of 80000 projections of the CitS protein indicated high numbers of elongated particles with a long axis approximately twice the length of the short axis. CitS appears to have two main types of projection views (Figure 3C,D). One appears to be a biscuit-shaped particle with a long axis of 160 Å and a short axis of 84 Å (Figure 3C). The second is a kidney-shaped particle with a long axis of the same length (160 Å) and a total height of 92 Å (Figure 3D). In the middle, the particle measures 78 Å. The two classes represent two views of the protein rotated around the long axis. Secondary transporter proteins are largely embedded in the phospolipid bilayer without too much of their mass protruding into the interior or exterior water phase. Considering that the thickness of the membrane layer is

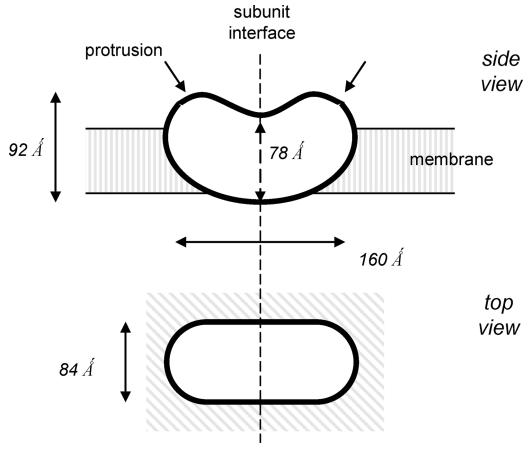


FIGURE 4: Model of the CitS dimer in the membrane. See the text for an explanation.

~40−50 Å, the long axis of both projections has to be in the plane of the membrane. Then, in the two projections, the short axis is either also in the plane of the membrane (view on the membrane, top view) or perpendicular to the membrane (view from within the membrane, side view). Since the orientation of an integral membrane protein in the membrane is fixed [positive inside rule (*34*)], a (homo)dimeric structure of a membrane protein forces certain symmetries upon the projections. In the side view projection, one-half should be the mirror image of the other half, which, in support for a dimeric structure of CitS, is observed for both projections. However, the top view should have 2-fold rotational symmetry (see the 3-fold rotational symmetry for the GltT trimer above) which is only compatible with the biscuit-shaped and not the kidney-shaped image. It follows that the kidney-shaped image (Figure 3D) represents the side view and the biscuit-shaped image the top view of the CitS dimer. The symmetry axes correspond to the subunit interface in the dimer. Figure 4 presents a model of the CitS dimer.

*(iii) GltS*. The sums of the best groups of classes from a set of 30000 EM projections of GltS are presented in panels E and F of Figure 3. As for CitS, mainly two types of projection views of GltS were found. The short axes of the projections were similar as observed for the top view image of CitS (84 Å), while the long axis was significantly shorter (145 Å vs. 160 Å). The difference in shape between the two main projections of the GltS particle is smaller than that observed for CitS (compare panels C and D of Figure 3 and panels E and F of Figure 3). The image shown in Figure 3E is somewhat asymmetric along the long axis, suggesting a slight tilt of particles out of the membrane plane. A small constriction in the middle of the projections seems to be present, suggesting similarity to the kidney-shaped projection of CitS in Figure 3D. Overall, the shape and size of the CitS and GltS particles are very similar and consistent with a dimeric structure for GltS.

## DISCUSSION

Single-particle EM analysis is not (yet) able to reveal much detail in membrane proteins with a mass of ~100 kDa because of the small dimensions, the unstructured detergent shell around the proteins, and the low signal-to-noise ratio of transmission EM images of biomacromolecules. Nevertheless, the studies of secondary transporters GltT, CitS, and GltS by electron microscopy and single-particle averaging reported here reveal several new insights into the architecture of these small proteins. The

$H^+$-glutamate transporter GltT found in the Gram-positive bacteria *B. stearothermophilus* and *Bacillus caldotenax* (*17*) appears to have the same overall structure as the homologous archaeal transporter $Glt_{Ph}$ of *P. horikoshii* for which a high-resolution crystal structure is available (*5*). The top view image of GltT presented here is the first EM projection structure of a particle as small as 140 kDa that is validated by an X-ray structure. The $Na^+$-citrate transporter CitS and the $Na^+$-glutamate transporter GltS found in *K. pneumoniae* and *E. coli*, respectively, are evolutionarily unrelated to GltT, and the images clearly demonstrate different overall shapes, indicating different structures. The images reveal 2-fold symmetry properties consistent with dimeric structures for CitS and GltS. The two main views obtained for the CitS particle allowed for discrimination between top and side views which allows for the reconstruction of the shape of the CitS dimer sitting in the membrane (Figure 4). It follows that it is feasible to obtain useful two-dimensional projection maps from dimers and trimers of small (40−50 kDa) membrane proteins by single-particle electron microscopy. Large numbers of projections, however, have to be processed. Where sets of ~1000 projections already may provide useful, trustworthy information for large membrane protein complexes, such as F- and V-type ATP synthases and photosystems I and II, sets containing 10−100 times more projections are required for the smaller proteins. With the recent progress in automated data aqcuisition and processing, this is in practice not a main drawback anymore (*35*).

In this study, a total of ~130000 projections of negatively stained GltT, CitS, and GltS transport proteins were analyzed by single-particle analysis and final class sums for all three particles were obtained (Figure 3). However, the number of processed projections, necessary to obtain consistent details in the projection maps, differed considerably between the three transporters. For GltT, a number of 5000 was sufficient, while for CitS and GltS, 80000 and 30000 were required, respectively. Several reasons may contribute to this difference. One, trimeric GltT is a larger particle than dimeric CitS or GltS. Two, for GltT, essentially only one type of projection was found showing particles in a top view position, parallel to the membrane plane. No side views were found. This may be caused by the glow-discharge treatment of the grids before preparation of electron microscopy specimens which enhances the absorption of particles with their hydrophilic parts. In the case of membrane proteins, this favors top view projections. Three, the top view projections of GltT have a distinct triangular shape, which helps tremendously in accurate averaging of small numbers of particles. We have found before that large membrane protein complexes that are oval-shaped (e.g., photosystem I) are much harder to analyze than rectangule-shaped complexes (e.g., the photosystem II supercomplex) (*36*). In the case of the former, several thousand particle projections are needed as a critical minimal number, whereas with the latter, already a couple of hundred particles give a reliable sum. The reason is that unless the accuracy of rotational alignments is within ~1−2°, the particle sums smear out. The combination of small size and the rather unpronounced overall shape of the CitS and GltS proteins required a much higher number of particles to obtain good classes. The criterion that a continuous and sharp border between the protein and the surrounding negative stain should be present after averaging was used. With initial sets of ~10000 particles, classes remained fuzzy. Hence, numbers were increased to 80000 and 30000, respectively.

Figure 4 presents a schematic of the CitS dimer sitting in the membrane based on the top view and side view images presented in panels C and D of Figure 3, respectively. In the side view, the CitS dimer would be a particle with a strongly curved surface at one side of the membrane and a clear indentation at the other side at the interface of the subunits. There is a remarkable similarity between the shape of the CitS dimer and the structure of the $Glt_{Ph}$ trimer of *P. horikoshii*, the space filling model of which is projected on the top view of the GltT image in Figure 3B. $Glt_{Ph}$, a $Na^+$-aspartate symporter, has a bowl-shaped architecture with an aqueous basin (the indentation in CitS) facing the extracellular water phase and significant protein mass protruding into the cytoplasm at the center of the complex where the three protomers meet (the strongly curved surface of CitS). Each of the subunits of $Glt_{Ph}$ contains a translocation pathway that is accessed by substrate and co-ions from the aqueous basin. The translocation pathways are gated by two re-entrant loops, one at each side of the membrane (*37*). Two re-entrant loops are also a prominent feature of structural models of the CitS monomer (*14*, *38*). Possibly, CitS represents a dimeric version of the gated secondary transporter mechanism demonstrated for trimeric $Glt_{Ph}$.

## REFERENCES


1. Saier, M. H., Jr. (2000) A functional-phylogenetic classification system for transmembrane solute transporters. *Microbiol. Mol. Biol. Rev. 64*, 354–411.
2. Abramson, J., Smirnova, I., Kasho, V., Verner, G., Kaback, H. R., and Iwata, S. (2003) Structure and mechanism of the lactose permease of *Escherichia coli*. *Science 301*, 610–615.
3. Huang, Y., Lemieux, M. J., Song, J., Auer, M., and Wang, D.-N. (2003) Structure and mechanism of the glycerol-3-phosphate transporter from *Escherichia coli*. *Science 301*, 616–620.
4. Murakami, S., Nakashima, R., Yamashita, E., and Yamaguchi, A. (2002) Crystal structure of bacterial multidrug efflux transporter AcrB. *Nature 419*, 587–593.
5. Yernool, D., Boudker, O., Jin, Y., and Gouaux, E. (2004) Structure of a glutamate transporter homologue from *Pyrococcus horikoshii*. *Nature 431*, 811–818.
6. Khademi, S., O'Connell, J.III, Remis, J., Robles-Colmenares, Y., Miercke, L. J. W., and Stroud, R. (2004) Mechanism of ammonia transport by Amt/MEP/Rh: Structure of AmtB at 1.35 Å. *Science 305*, 1587–1594.
7. Hunte, C., Screpanti, E., Venturi, M., Rimon, A., Padan, E., and Michel, H. (2005) Structure of a $Na^+/H^+$ antiporter and insights into mechanism of action and regulation by pH. *Nature 435*, 1197–1202.
8. Yamashita, A., Singh, S. K., Kawate, T., Jin, Y., and Gouaux, E. (2005) Crystal structure of a bacterial homologue of the $Na^+/Cl^-$-dependent neurotransmitter transporters. *Nature 437*, 215–223.
9. Faham, S., Watanabe, A., Mercado Bessemer, G., Cascio, D., Szpecht, A., Hirayama, B. A., Wright, E. M., and Abramson, J. (2008) The crystal structure of a sodium galactose transporter reveals mechanistic insights into $Na^+$/sugar symport. *Science 321*, 810–814.
10. Weyand, S., Shimamura, T., Yajima, S., Suzuki, S., Mirza, O., Krusong, K., Carpenter, E. P., Rutherford, N. G., Hadden, J. M., O'Reilly, J., Ma, P., Saidijam, M., Patching, S. G., Hope, R. J., Norbertczak, H. T., Roach, P. C., Iwata, S., Henderson, P. J., and Cameron, A. D. (2008) Structure and molecular mechanism of a nucleobase-cation-symport-1 family transporter. *Science 322*, 709–713.
11. Frank, J. (2002) Single-particle imaging of macromolecules by cryo-electron microscopy. *Annu. Rev. Biophys. Biomol. Struct. 31*, 309–319.
12. van Heel, M., Gowen, B., Matadeen, R., Orlova, E. V., Finn, R., Pape, T., Cohen, D., Stark, H., Schmidt, R., Schatz, M., and Patwardhan, A. (2000) Single-particle electron cryo-microscopy: Towards atomic resolution. *Q. Rev. Biophys. 33*, 307–369.
13. Slotboom, D. J., Koning, W. N., and Lolkema, J. S. (1999) Structural features of the glutamate transporter family. *Microbiol. Mol. Rev. 63*, 293–307.
14. Sobczak, I., and Lolkema, J. S. (2005) The 2-hydroxycarboxylate transporter family: Physiology, structure, and mechanism. *Microbiol. Mol. Biol. Rev. 69*, 665–695.

15. Kalman, M., Gentry, D. R., and Cashel, M. (1991) Characterization of the *Escherichia coli* K12 gltS glutamate permease gene. *Mol. Gen. Genet. 225*, 379–386.
16. Deguchi, Y., Yamato, I., and Anraku, Y. (1990) Nucleotide sequence of gltS, the $Na^+$/glutamate symport carrier gene of *Escherichia coli* B. *J. Biol. Chem. 265*, 21704–21708.
17. Tolner, B., Poolman, B., and Konings, W. N. (1992) Characterization and functional expression in *Escherichia coli* of the sodium/proton/glutamate symport proteins of *Bacillus stearothermophilus* and *Bacillus caldotenax*. *Mol. Microbiol. 6*, 2845–2856.
18. Lolkema, J. S., and Slotboom, D. J. (1998) Estimation of structural similarity of membrane proteins by hydropathy profile alignment. *Mol. Membr. Biol. 15*, 33–42.
19. Lolkema, J. S., and Slotboom, D. J. (2003) Classification of 29 families of secondary transport proteins into a single structural class using hydropathy profile analysis. *J. Mol. Biol. 327*, 901–909.
20. Dobrowolski, A., Sobczak-Elbourne, I., and Lolkema, J. S. (2007) Membrane Topology Prediction by Hydropathy Profile Alignment: Membrane Topology of the $Na^+$-Glutamate Transporter GltS. *Biochemistry 46*, 2326–2332.
21. Dobrowolski, A., and Lolkema, J. S. (2009) Functional importance of GGXG sequence motifs in putative pore-loop structures of 2HCT and ESS. *Biochemistry* (in press).
22. Yernool, D., Boudker, O., Folta-Stogniew, E., and Gouaux, E. (2003) Trimeric subunit stoichiometry of the glutamate transporters from *Bacillus caldotenax* and *Bacillus stearothermophilus*. *Biochemistry 42*, 12981–12988.
23. Groeneveld, M., and Slotboom, D. J. (2007) Rigidity of the subunit interfaces of the trimeric glutamate transporter GltT during translocation. *J. Mol. Biol. 372*, 565–570.
24. Pos, K. M., Bott, M., and Dimroth, P. (1994) Purification of two active fusion proteins of the $Na^+$-dependent citrate carrier of *Klebsiella pneumoniae*. *FEBS Lett. 347*, 37–41.
25. Veenhoff, L. M., Heuberger, E. H. M. L., Duurkens, H. H., and Poolman, B. (2001) Oligomeric state of membrane transport proteins analyzed with blue native electrophoresis and analytical ultracentrifugation. *J. Mol. Biol. 317*, 591–600.
26. Kästner, C. N., Prummer, M., Sick, B., Renn, A., Wild, U. P., and Dimroth, P. (2003) The citrate carrier CitS probed by single-molecule fluorescence spectroscopy. *Biophys. J. 84*, 1651–1659.
27. Slotboom, D. J., Sobczak, I., Konings, W. N., and Lolkema, J. S. (1999) A conserved serine-rich stretch in the glutamate transporter family forms a substrate-sensitive reentrant loop. *Proc. Natl. Acad. Sci. U.S.A. 96*, 14282–14287.
28. Sobczak, I., and Lolkema, J. S. (2003) Accessibility of cysteine residues in a cytoplasmic loop of CitS of *Klebsiella pneumoniae* is controlled by the catalytic state of the transporter. *Biochemistry 42*, 9789–9796.
29. Laemmli, U. K. (1970) Cleavage of structural proteins during the assembly of the head of bacteriophage T4. *Nature 227*, 680–685.
30. Wittig, I., Braun, H. P., and Schägger, H. (2006) Blue native PAGE. *Nat. Protoc. 1*, 418–428.
31. Penczek, P., Radermacher, M., and Frank, J. (1992) Three dimensional reconstruction of single particles embedded in ice. *Ultramicroscopy 40*, 33–53.
32. Van Heel, M. (1987) Similarity measures between images. *Ultramicroscopy 21*, 95–100.
33. Boekema, E. J., van Roon, H., van Breemen, J. F. L., and Dekker, J. P. (1999) Supramolecular organization of photosystem II and its light-harvesting antenna in partially solubilized photosystem II membranes. *Eur. J. Biochem. 266*, 444–452.
34. von Heijne, G. (1989) Control of topology and mode of assembly of a polytopic membrane protein by positively charged residues. *Nature 341*, 456–458.
35. Stagg, S. M., Lander, G. C., Pulokas, J., Fellmann, D., Cheng, A., Quispe, J. D., Mallick, S. P., Avila, R. M., Carragher, B., and Potter, C. S. (2006) Automated cryoEM data acquisition and analysis of 284,742 particles of GroEL. *J. Struct. Biol. 155*, 470–481.
36. Kouřil, R., Zygadlo, A., Arteni, A. A., de Wit, C. D., Dekker, J. P., Jensen, P. E., Scheller, H. V., and Boekema, E. J. (2005) Structural characterization of a complex of photosystem I and light-harvesting complex II of *Arabidopsis thaliana*. *Biochemistry 44*, 10935–10940.
37. Boudker, O., Ryan, R. M., Yernool, D., Shimamoto, K., and Gouaux, E. (2007) Coupling substrate and ion binding to extracellular gate of a sodium-dependent aspartate transporter. *Nature 445*, 387–393.
38. Sobczak, I., and Lolkema, J. S. (2004) Alternate access and a pore-loop structure in the $Na^+$-citrate transporter CitS of *Klebsiella pneumoniae*. *J. Biol. Chem. 279*, 31113–31120.